Editors' Suggestion

Exploring the Regime of Fragmentation in Strongly Tilted Fermi-Hubbard Chains

Thomas Kohlert,[1,2,3] Sebastian Scherg,[1,2,3] Pablo Sala[ORCID],[3,4] Frank Pollmann,[3,4] Bharath Hebbe Madhusudhana,[1,2,3] Immanuel Bloch,[1,2,3] and Monika Aidelsburger[ORCID][1,3,*]

[1]*Fakultät für Physik, Ludwig-Maximilians-Universität München, 80799 Munich, Germany*
[2]*Max-Planck-Institut für Quantenoptik, 85748 Garching, Germany*
[3]*Munich Center for Quantum Science and Technology (MCQST), 80799 Munich, Germany*
[4]*Department of Physics and Institute for Advanced Study, Technical University of Munich, 85748 Garching, Germany*

Intriguingly, quantum many-body systems may defy thermalization even without disorder. One example is so-called fragmented models, where the many-body Hilbert space fragments into dynamically disconnected subspaces that are not determined by the global symmetries of the model. In this Letter we demonstrate that the tilted one-dimensional Fermi-Hubbard model naturally realizes distinct effective Hamiltonians that are expected to support nonergodic behavior due to fragmentation, even at resonances between the tilt energy and the Hubbard on site interaction. We find that the effective description captures the observed dynamics in experimentally accessible parameter ranges of moderate tilt values. Specifically, we observe a pronounced dependence of the relaxation dynamics on the initial doublon fraction, which directly reveals the microscopic processes of the fragmented model. Our results pave the way for future studies of nonergodic behavior in higher dimensions.

Quantum many-body systems out of equilibrium are typically characterized according to their long-time behavior of local observables. While generic quantum systems reach thermal equilibrium as predicted by the eigenstate thermalization hypothesis (ETH) [1–3], well-known exceptions to this paradigm are integrable [4,5] and many-body localized (MBL) systems [6–10]. Their nonergodicity is based on an extensive set of conserved quantities [11,12]. Recently, a new class of models with intermediate behavior, summarized as weak ergodicity breaking [13], renewed the interest in questions of quantum thermalization. A key signature of weak ergodicity breaking is the strong dependence of the dynamics on the initial conditions, which discriminates it from both fully thermal and strongly ergodicity-breaking systems. This is due to a special structure of the many-body Hilbert space, which exhibits (approximately) disconnected subspaces that are not characterized by the global symmetries of the model.

For instance, quantum many-body scars [14–20], as recently observed with Rydberg atoms [21,22], are the result of an atypical set of eigenstates, which are embedded in an otherwise thermal spectrum. Another prominent example are fractonic systems, such as one dimensional (1D) setups with conserved U(1) charge and its associated dipole moment [23–27]. In these models the Hilbert space fragments into exponentially many disconnected subspaces, a phenomenon known as *Hilbert-space fragmentation*. In fact, similar phenomena also appear in classical stochastic dynamics in the realm of kinetically constrained spin systems, where it is known as reducibility [28,29]. The major difference is that

dipole and higher-moment conserving systems [29] provide a provable and systematic way of constructing such models without explicit kinetic constraints.

Remarkably, the tilted 1D Fermi-Hubbard model [Fig. 1(a)] exhibits a wide range of (weak) ergodicity-breaking phenomena and has emerged as a versatile platform for experimental studies of nonergodicity. Recent experiments have studied the low-tilt regime investigating disorder-free localization in the form of Stark MBL with ions [30] and superconducting qubits [31], as well as nonergodicity due to kinetic constraints using ultracold fermions in tilted optical lattices [32]. Intriguingly, in the limit of strong tilts $\Delta \gg J$, the Fermi-Hubbard model hosts a variety of distinct fragmented models, which are derived as effective Hamiltonian descriptions [23–25]. In this regime, approximate conservation laws, such as dipole-moment conservation, result in a fragmentation of the Hilbert space into exponentially many fragments $\mathcal{K}$, such that even states belonging to the same symmetry sector $\mathcal{S}$, defined, e.g., by the dipole moment, may become dynamically disconnected [Fig. 1(b)], when considering finite order in perturbation theory. In this Letter we experimentally study the properties of the underlying effective Hamiltonian that governs the transient dynamics. We study the relaxation dynamics of a period-two charge density wave up to about 140 tunneling times for different doublon (doubly occupied site) fractions n_D [Fig. 1(c)] in the initial state. We observe distinct relaxation behavior for different initial states, whose microscopic origin is at the heart of Hilbert-space fragmentation in the tilted Fermi-Hubbard model.
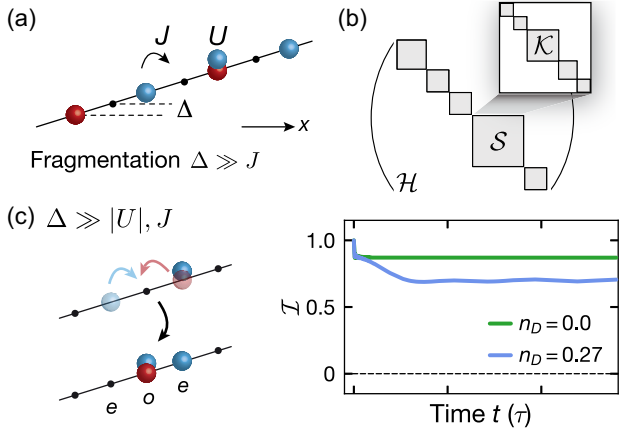
FIG. 1. Hilbert-space fragmentation in the tilted 1D Fermi Hubbard model. (a) Schematic of the tilted Fermi-Hubbard model (↑ atoms red, ↓ atoms blue) with linear potential ("tilt") of strength Δ, tunneling J, and Hubbard interaction U. (b) Schematic illustration of Hilbert-space fragmentation. The symmetry sectors $\mathcal{S}$ of the total Hilbert space $\mathcal{H}$ decouple into (approximately) disconnected fragments $\mathcal{K}$. (c) Doublon-number dependent relaxation dynamics $\mathcal{I}(t)$ starting from an initial period-two charge-density wave with $\mathcal{I}(0) = 1$ and doublon fraction n_D. The imbalance $\mathcal{I}$ is a measure for the relative occupation of even e and odd o lattice sites; τ is one tunneling time. The schematic illustrates the correlated tunneling process of the effective Hamiltonian for $\Delta \gg |U|, J$ [Eq. (2)], which dominates, when the initial state contains doublons ($n_D > 0$). The solid lines are TEBD simulations (cumulative average) for $U = 2.7J$ and $\Delta = 8J$ for a lattice with $L = 101$ ($n_D = 0$) and $L = 52$ ($n_D = 0.27$) sites according to the effective Hamiltonian [Eq. (2)]. The dashed line indicates the steady-state value of $\mathcal{I}$ for a thermal system at infinite temperature (within $\mathcal{S}$).

Our experimental setup consists of a degenerate Fermi gas of about $50(5) \times 10^3$ ^{40}K atoms at an average temperature of $0.12(2)T_F$, where T_F is the Fermi temperature. The gas is prepared in an equal mixture of two magnetic hyperfine states, $|\downarrow\rangle = |m_F = -9/2\rangle$ and $|\uparrow\rangle = |m_F = -7/2\rangle$, in the $F = 9/2$ ground-state hyperfine manifold. The fermions are loaded into a 3D optical lattice created by three pairs of retroreflected laser beams. The lattice along the primary axis has a wavelength $\lambda_p = 532$ nm, and the orthogonal lattices operate at $\lambda_\perp = 738$ nm. We work at a primary lattice depth of $12E_{r,p}$, where one tunneling time $\tau = \hbar/J = 0.75$ ms. The orthogonal lattices are set to $55E_{r,\perp}$; here $E_{r,i} = h^2/(2m\lambda_i^2)$ is the recoil energy, with $i \in \{p, \perp\}$, m the atomic mass, λ_i the respective lattice wavelength, and h the Planck constant. This creates a 2D array of 1D chains, where the central chain has a length $L \approx 290$ and coupling to neighboring chains is suppressed by a factor of $\sim 10^{-3}$, such that the system can be considered 1D on our experimental timescales. A magnetic field generated via a single coil induces a linear potential gradient ("tilt") along the primary lattice axis. Since the spins are encoded in different magnetic hyperfine states, the

tilt Δ_σ, $\sigma \in \{\uparrow, \downarrow\}$, is slightly state dependent, $\Delta_\uparrow \simeq 0.9\Delta_\downarrow$ [33]. The dynamics of each 1D chain is described by the tilted 1D Fermi-Hubbard model [Fig. 1(a)]

$$\hat{H} = -J\sum_{i,\sigma}(\hat{c}^\dagger_{i+1,\sigma}\hat{c}_{i,\sigma} + \text{H.c.}) + U\sum_i \hat{n}_{i,\uparrow}\hat{n}_{i,\downarrow}$$
$$+ \sum_{i,\sigma}\Delta_\sigma i\hat{n}_{i,\sigma}, \qquad (1)$$

where $\hat{c}_{i,\sigma}$ ($\hat{c}^\dagger_{i,\sigma}$) denotes the fermionic annihilation (creation) operator for spin σ on site i and $\hat{n}_i = \hat{c}^\dagger_i\hat{c}_i$.

In order to study dynamics, we use a bichromatic superlattice to prepare a period-two charge-density wave (CDW), where only even sites are occupied [33]. After a short dephasing time in the deep 3D lattice there are no residual coherences, and the initial state can be described by an incoherent mixture of localized product states with random spin configurations at zero net magnetization. The dynamics is initiated by quenching the primary lattice to the desired value. After initiating the dynamics, we probe the relaxation by measuring the relative atom number on even (N_e) and odd (N_o) lattice sites, given by the ensemble-averaged imbalance $\mathcal{I} = (N_e - N_o)/(N_e + N_o)$, which we directly extract using a bandmapping technique [49,50]. Moreover, using near-resonant light pulses to remove doubly occupied sites before detection, we have access to singlon (singly occupied site) and doublon-resolved imbalances, $\mathcal{I}_S$ and $\mathcal{I}_D$. In this Letter we restrict our observation times to 140τ, since for longer times light-assisted collisions significantly reduce the doublon fraction [33].

In the limit of large tilts $\Delta \gg |U|, J$ and for $\Delta \equiv \Delta_\downarrow = \Delta_\uparrow$ we can use a Schrieffer-Wolff (SW) transformation to expand Hamiltonian [Eq. (1)] in powers of $1/\Delta$ [33]. Up to third order it reads as

$$\hat{H}_{\text{eff}} = J^{(3)}(\hat{T}_3 + 2\hat{T}_{XY} + 2\hat{V}) + \tilde{U}\sum_i \hat{n}_{i,\uparrow}\hat{n}_{i,\downarrow}, \qquad (2)$$

with the effective tunneling $J^{(3)} = J^2U/\Delta^2$, the renormalized on site Hubbard interaction $\tilde{U} = U(1 - 4J^2/\Delta^2)$, and a nearest-neighbor interaction $\hat{V} = \sum_{i,\sigma} \hat{n}_{i,\sigma}\hat{n}_{i+1,\bar{\sigma}}$, where $\bar{\sigma}$ denotes the opposite spin of σ. The dynamics is governed by $\hat{T}_3 = \sum_{i,\sigma}(\hat{c}^\dagger_{i,\sigma}\hat{c}_{i+1,\sigma}\hat{c}_{i+1,\bar{\sigma}}\hat{c}^\dagger_{i+2,\bar{\sigma}} + \text{H.c.})$ and an exchange term $\hat{T}_{XY} = \sum_i(\hat{c}^\dagger_{i,\uparrow}\hat{c}_{i,\downarrow}\hat{c}^\dagger_{i+1,\downarrow}\hat{c}_{i+1,\uparrow} + \text{H.c.})$. This Hamiltonian is SU(2) invariant and conserves charge ($\hat{Q} = \sum_i \hat{n}_i$) and dipole moment ($\hat{P} = \sum_i i\hat{n}_i$). Similar to other dipole-conserving models studied previously in spin chains [23], random unitary circuits [24,26], and spinless Hubbard systems [25,27], it is strongly fragmented.

The spin-dependent tilt Δ_σ in Hamiltonian [Eq. (1)] introduces additional constraints. In order to tune this spin-dependence in the experiment we employ the technique of radio-frequency (RF) dressing [33,51,52], where we use an
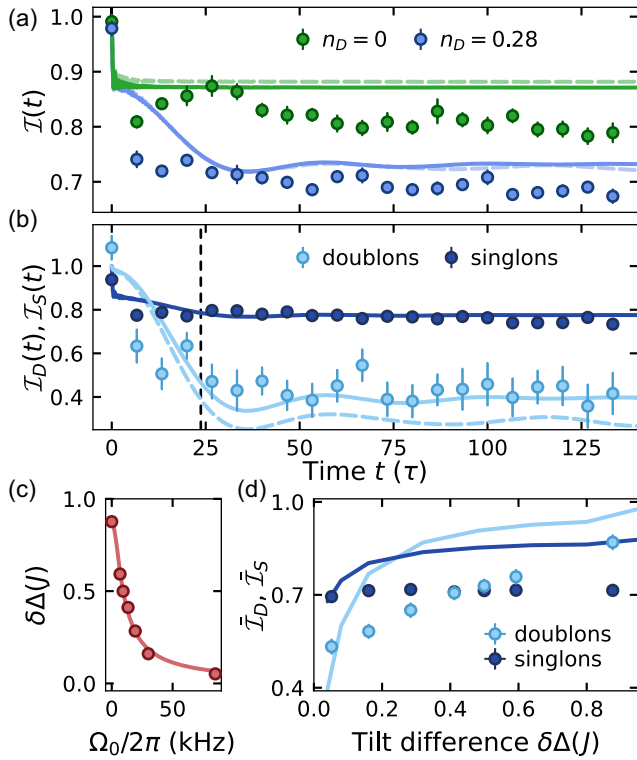
FIG. 2. Effective Hamiltonian dynamics for $\Delta \gg |U|, J$. (a) Imbalance time trace for singlon ($n_D \simeq 0$) and mixed [$n_D = 0.28(2)$] CDW initial states for $\Delta/J = 8.0(2)$, $U/J = 2.7(2)$, and $\delta\Delta = 0.048J$ [resonant Rabi frequency $\Omega_0 = 85(1)$ kHz]. (b) Singlon- and doublon-resolved imbalance for the mixed initial state [$n_D = 0.28(2)$] for the same parameters. The lines in (a) and (b) are time-averaged TEBD simulations with $L = 101$ lattice sites with the exact (dashed, transparent lines) and the effective model (solid lines) including a hole fraction of 20% (comparable to Ref. [54]). The dashed vertical line shows the effective timescale $1/(2\pi J^{(3)})$. Experimental data points are averaged 10 times, and error bars are the standard error of the mean (SEM). (c) Relative tilt difference $\delta\Delta$ as a function of the resonant Rabi frequency Ω_0 in the presence of the RF dressing field. The solid line is a fit of the analytic model defined in Eq. (S4). (d) Steady-state imbalance averaged over ten data points between 67τ and 80τ as a function of the tilt difference between both spins for $\Delta/J = 8.0(2)$, $U/J = 2.7(2)$, and $n_D = 0.47(4)$. Solid lines of the same color as the data points are TEBD simulations with the exact Hamiltonian [Eq. (1)] on 101 lattice sites, $n_D = 0.46$ and a hole fraction of 20% (TEBD simulations in all panels include averaging over the spatial distribution of $\delta\Delta$). See Table S1 in Ref. [33] for numerical details.

additional RF field to couple the two spins. Thereby we realize dressed states that see a weighted average of $\Delta_\uparrow$ and $\Delta_\downarrow$. The weights are determined by the resonant RF coupling strength Ω_0 and the detuning from resonance. This allows us to adjust the relative tilt difference $\delta\Delta = (\tilde{\Delta}_\downarrow - \tilde{\Delta}_\uparrow)$ by tuning the RF coupling strength [Fig. 2(c)], where $\tilde{\Delta}_\sigma$ denotes the spin-dependent tilt of the dressed states. The maximum tilt difference is determined by the

m_F quantum numbers in the absence of RF dressing, and the smallest value of $\delta\Delta = 0.048J$ is reached for the largest coupling strength. The Hubbard interaction U is invariant under RF dressing [33,53], which allows us to tune its magnitude via the Feshbach resonance at 202.1 G. There is also a residual harmonic confinement due to the trapping laser beams. The strength of this term is $\sim 10^{-3}J$ and does not impact the steady-state behavior on the timescales studied in this Letter, as shown previously [32].

We start by measuring relaxation dynamics for initial states with and without doublons [Fig. 2(a)], where $n_D = N_D/(N_S + N_D)$ and N_D (N_S) is the number of atoms on doubly (singly) occupied lattice sites [33]. After a fast drop at short times, a steady-state value emerges for evolution times $t > 30\tau$, hinting toward nonergodic behavior. The apparent fast drop develops during coherent Bloch oscillations at short times, which we do not study here. For initial states with doublons the steady-state value is reduced, in agreement with time-evolving block decimation (TEBD) simulations [33] of the full [Eq. (1)] and the effective model [Eq. (2)]. Here, the numerical traces are time averaged [Figs. 2(a) and 2(b)] in order to mimic dephasing of the observed oscillations, which in the experiment is realized by averaging over an inhomogeneous distribution. In the Supplemental Material [33], we provide an extensive discussion of different imperfections in our system. We find that the observed dynamics shows a remarkable resilience to most of them, and we only included the relevant ones in the theoretical model, which we identified as the fraction of holes in the initial state and averaging over the residual spin-dependent tilt $\delta\Delta$. The slow residual decay of the experimental singlon time trace is due to technical heating caused by the transverse lattice laser beams. The exact and effective numerical traces are in agreement. The small systematic offset for $t \gtrsim 10\tau$ is due to higher order terms and decreases for larger tilts or smaller interactions.

The effective model in Eq. (2) allows for a microscopic understanding of the doublon-dependent dynamics. This is best revealed in the singlon- and doublon-resolved imbalance traces [Fig. 2(b)]. Starting from a period-two CDW with $\mathcal{I}(0) = 1$, there is only one correlated tunneling process governed by $\hat{T}_3$, that can initiate the dynamics [schematics in Fig. 1(c)]. For pure singlon initial states this process is energetically suppressed by the effective on site interaction energy $\tilde{U}$, since in the large-tilt limit $J^{(3)}/\tilde{U} \simeq (J/\Delta)^2 \ll 1$. The presence of doublons, however, renders this process resonant, which is expected to relax the CDW on a timescale governed by the hopping rate $J^{(3)}$. Indeed we find that while the singlon imbalance $\mathcal{I}_S$ remains stable even for mixed initial states, there is a pronounced decrease of the doublon imbalance $\mathcal{I}_D$. This is due to $\hat{T}_3$ [Fig. 1(c)], which leads to a fast rearrangement of doublons between even and odd lattice sites on a timescale

$1/(2\pi J^{(3)}) \simeq 24\tau$, while keeping the singlon configuration fixed.

Experimentally, we further explore the effect of SU(2) symmetry breaking on the observed singlon- and doublon-resolved steady-state values by tuning the tilt difference $\delta\Delta$ [Fig. 2(d)]. We consider the regime $J > |\tilde{\Delta}_\uparrow - \tilde{\Delta}_\downarrow|$, where the perturbative description [Eq. (2)] remains valid. For $|\tilde{\Delta}_\uparrow - \tilde{\Delta}_\downarrow| > 0$, the relevant process enabled by $\hat{T}_3$ is energetically detuned even in the presence of doublons, and we expect relaxation to be strongly suppressed for $|\tilde{\Delta}_\uparrow - \tilde{\Delta}_\downarrow| > J^{(3)}$. This is supported by the observed dependence of the doublon dynamics on the tilt difference. The signal obtained from the singlons on the other hand shows no significant dependence. For $|\tilde{\Delta}_\uparrow - \tilde{\Delta}_\downarrow| > J^{(3)}$ there is an intuitive description of the doublon steady-state imbalance in terms of a Wannier-Stark localized doublon-hole pair, which agrees well with the numerical simulations [33]. While the general trend observed in the experiment is reproduced by TEBD simulations, there is a systematic deviation for large $\delta\Delta$, which we attribute to technical heating induced by the transverse lattice laser beams, that mostly affects large imbalance values and mixed initial states.

The tilted 1D Fermi-Hubbard model exhibits rich nonergodic phenomena depending on its microscopic parameters, including emergent Hilbert-space fragmentation and quantum scars. We study the doublon-dependent dynamics over a wide range of parameters by measuring the intermediate-time steady-state imbalance as a function of the Hubbard interaction strength for $\tilde{\Delta}_\uparrow \simeq \tilde{\Delta}_\downarrow$ [Fig. 3(a)]. We find that pure singlon initial states show no significant dependence. Initial states with doublons on the other hand, show a strong interaction as well as doublon-number dependent behavior, in particular near resonances between the tilt and interaction energy [55]. Intuitively, one may expect that away from the dipole-conserving regime ($\Delta \gg J, |U|$) the tilted Fermi-Hubbard model is ergodic due to the many resonances between the interaction U and the tilt energy Δ. Surprisingly, we find that the intermediate-time steady state persists over large parameter ranges. Indeed, strongly fragmented Hamiltonians have been derived for special resonant points in the parameter space: $|U| \simeq 2\Delta$ [33] and $|U| \simeq \Delta$ [56].

On the double-tilt resonance ($|U| \simeq 2\Delta$) fragmentation is due to the conservation of dipole moment and doublon number: $\Delta\hat{P} + U\sum_i \hat{n}_{i,\uparrow}\hat{n}_{i,\downarrow}$. As before we compare the dynamics of initial states with and without doublons [Fig. 3(b)]. We find a large reduction of the steady-state imbalance for $n_D > 0$, similar to the results shown in Fig. 2(a). However, unlike in the previous regime, the singlon- and doublon-resolved imbalance time traces exhibit similar dynamics, as expected based on the microscopic processes of the effective Hamiltonian.
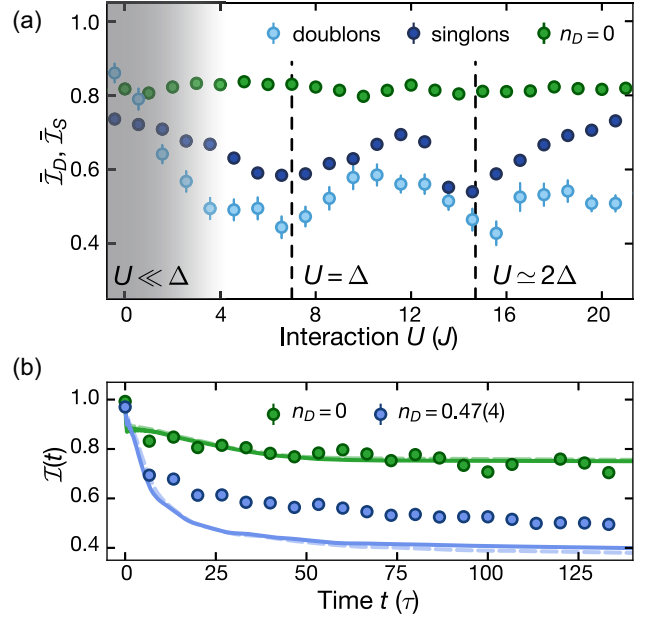

FIG. 3. Doublon-dependent dynamics for various interaction strengths and $\Delta/J = 8.0(2)$. (a) Steady-state singlon and doublon imbalance for $n_D = 0.47(4)$ and $\delta\Delta = 0.048J$ averaged over $t \in [67\tau, 80\tau]$. For comparison we also show the singlon initial state ($n_D \simeq 0$). The dashed vertical lines and the gray-shaded area highlight different regimes, where fragmented models have been found (main text). Data points contain eight averages over five points in time. Error bars are the SEM. (b) Imbalance time traces at the resonance $U = 14.7(2)J \simeq 2\Delta$ for a singlon initial state and with doublon fraction $n_D = 0.47(4)$. The resonance is chosen as the local minimum of $\bar{\mathcal{I}}_S$ in (a) as indicated by the vertical dashed line. Error bars denote the SEM after ten averages. The lines represent time-averaged TEBD simulations of the effective (solid) and the exact Hamiltonian (dashed, transparent) for $L = 51$, $n_D = 0.46$, and a hole fraction of 20% (See Table S1 in the Supplemental Material [33] for numerical details).

The fragmented structure of the many-body Hilbert space [Fig. 1(b)] naturally calls for a modified definition of ETH, where thermalization is defined not only with respect to a symmetry sector $\mathcal{S}$ but also to a particular fragment $\mathcal{K}$ (also known as Krylov-restricted thermalization). Within this modified framework the usual characteristics for identifying nonergodic behavior within a fragment apply [25,57]. In this Letter, we have studied the intermediate-time steady-state imbalance as a function of the fraction of doublons in the initial state in two regimes, where emergent fragmented models exist: the regime $\Delta \gg J, |U|$ [Fig. 4(a)] and the double-tilt resonance, where $|U| \simeq 2\Delta$ [Fig. 4(b)]. Note that initial states with different n_D belong to different symmetry sectors $\mathcal{S}$. In both regimes numerical simulations based on the effective Hamiltonian indicate that the steady-state value $\bar{\mathcal{I}}$ decreases with increasing doublon fraction (for $n_D < 0.5$), as confirmed by our experimental results. The system further relaxes to a
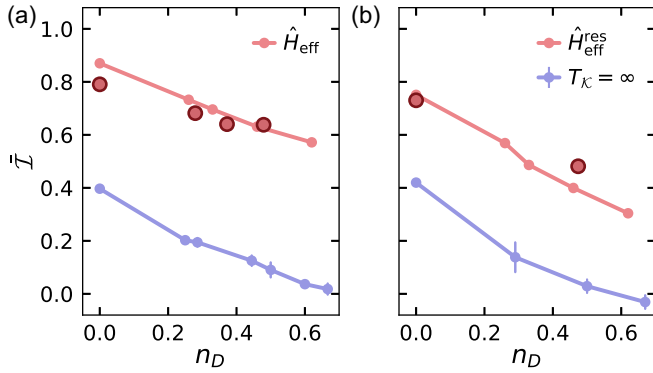
FIG. 4. Steady-state imbalance and infinite-temperature prediction. The data points (big red dots) show the steady-state imbalance for $\delta\Delta = 0.048J$ and $\Delta/J = 8.0(2)$, averaged between 120τ and 140τ as a function of n_D in the regime (a) $\Delta \gg J, |U|$ with $U/J = 2.7(2)$ and (b) $U = 14.7(2)J \simeq 2\Delta$. Averaging has been done using four points in time, and the error bars denote the respective SEM. Solid red lines are TEBD simulations (linear interpolation between numerical data points) with the effective Hamiltonians [Eq. (2) in (a) and $\hat{H}_{\text{eff}}^{\text{res}}$ in Eq. (S12) in (b)] with $L = 51$ and a hole fraction of 20%. The transparent blue lines (linear interpolation between numerical data points) show infinite-temperature predictions ($T_{\mathcal{K}} = \infty$) within the fragment $\mathcal{K}$ of the respective initial state calculated using exact diagonalization on 13, 15 and 17 lattice sites (without SW rotation of the initial state). (See Table S1 in the Supplemental Material [33] for numerical details).

finite value in contrast to ergodic systems thermalizing to infinite temperature within the symmetry sector $\mathcal{S}$, where $\mathcal{I}(\infty) = 0$. Moreover, the steady-state value $\bar{\mathcal{I}}$ does not agree with the infinite-temperature prediction for thermalization within the corresponding fragments (blue curve). Thus, in both regimes the numerical calculation (red curve) as well as the experimental data points indicate that the system does not thermalize to an infinite-temperature state up to 140τ. We emphasize that in general the dynamics within one fragment can be further constrained and exhibit nonergodic behavior [25], so *a priori* we do not know if the system would display thermal behavior even within this subspace. For instance, additional constraints have recently been identified in the resonant regime $|U| \simeq \Delta$ [56].

In conclusion, we have demonstrated that the tilted Fermi-Hubbard model constitutes an experimentally accessible platform to study the intriguing properties of Hilbert-space fragmentation. Even for intermediate values of the tilt as studied in this Letter, the dynamics is well captured by effective perturbative Hamiltonians that support the phenomenon of fragmentation. We have studied non-equilibrium dynamics in two specific regimes, where fragmentation has been shown theoretically ($\Delta \gg J, |U|$ and the resonant regime $|U| \simeq 2\Delta$). At the same time we find no experimental evidence for ergodic behavior away from these perturbative limits as long as Δ is significant

compared with J. We further demonstrate that the observed dependence of the dynamics on the number of doublons in the initial state is directly related to the microscopic processes of the effective Hamiltonian. It will be interesting to further systematically explore thermalization within individual fragments for the various different parameter regimes of the tilted Fermi-Hubbard model. Moreover, to reveal the fragmented nature of the spectrum more directly, one could further look at the thermalization of different initial states within the same symmetry sector $\mathcal{S}$. Moreover, at the resonance $|U| \simeq \Delta$ it was found that additional constraints result in scarring [56], which highlights the potential of this experimental platform for studying the interplay of both phenomena. Additionally, it is expected that higher-order terms in the perturbative expansion will generally lead to thermalization. However, because of the small amplitude of the higher-order terms even weak disorder or inhomogeneities can render these terms inefficient, which results in an interesting interplay between thermalization and localization connecting to the phenomenon of Stark-MBL [58,59]. The RF-dressing technique may further pave the way toward the implementation of effective spin models via precise control over the tilt difference. Intriguingly, by extending our system to 2D, we should be able to connect our studies to the emergence of hydrodynamic behavior [60] and potentially realize higher-dimensional models with multipole moment conservation [24,59].

*Corresponding author.
monika.aidelsburger@physik.uni-muenchen.de

[1] J. M. Deutsch, Quantum statistical mechanics in a closed system, Phys. Rev. A **43**, 2046 (1991).
[2] M. Srednicki, Chaos and quantum thermalization, Phys. Rev. E **50**, 888 (1994).

[3] M. Rigol, V. Dunjko, and M. Olshanii, Thermalization and its mechanism for generic isolated quantum systems, Nature (London) **452,** 854 (2008).

[4] P. Calabrese, F. H. L. Essler, and M. Fagotti, Quantum Quench in the Transverse-Field Ising Chain, Phys. Rev. Lett. **106,** 227203 (2011).

[5] F. H. L. Essler and M. Fagotti, Quench dynamics and relaxation in isolated integrable quantum spin chains, J. Stat. Mech. (2016) 064002.

[6] M. Schreiber, S. S. Hodgman, P. Bordia, H. P. Lüschen, M. H. Fischer, R. Vosk, E. Altman, U. Schneider, and I. Bloch, Observation of many-body localization of interacting fermions in a quasirandom optical lattice, Science **349,** 842 (2015).

[7] I. V. Gornyi, A. D. Mirlin, and D. G. Polyakov, Interacting Electrons in Disordered Wires: Anderson Localization and Low-T Transport, Phys. Rev. Lett. **95,** 206603 (2005).

[8] D. Basko, I. Aleiner, and B. Altshuler, Metalinsulator transition in a weakly interacting many-electron system with localized single-particle states, Ann. Phys. (Amsterdam) **321,** 1126 (2006).

[9] R. Nandkishore and D. A. Huse, Many-body localization and thermalization in quantum statistical mechanics, Annu. Rev. Condens. Matter Phys. **6,** 15 (2015).

[10] D. A. Abanin, E. Altman, I. Bloch, and M. Serbyn, Colloquium: Many-body localization, thermalization, and entanglement, Rev. Mod. Phys. **91,** 021001 (2019).

[11] M. Serbyn, Z. Papić, and D. A. Abanin, Local Conservation Laws and the Structure of the Many-Body Localized States, Phys. Rev. Lett. **111,** 127201 (2013).

[12] D. A. Huse, R. Nandkishore, and V. Oganesyan, Phenomenology of fully many-body-localized systems, Phys. Rev. B **90,** 174202 (2014).

[13] M. Serbyn, D. A. Abanin, and Z. Papić, Quantum many-body scars and weak breaking of ergodicity, Nat. Phys. **17,** 675 (2021).

[14] C. J. Turner, A. A. Michailidis, D. A. Abanin, M. Serbyn, and Z. Papić, Weak ergodicity breaking from quantum many-body scars, Nat. Phys. **14,** 745 (2018).

[15] C. J. Turner, A. A. Michailidis, D. A. Abanin, M. Serbyn, and Z. Papić, Quantum scarred eigenstates in a Rydberg atom chain: Entanglement, breakdown of thermalization, and stability to perturbations, Phys. Rev. B **98,** 155134 (2018).

[16] C. Chen, F. Burnell, and A. Chandran, How Does a Locally Constrained Quantum System Localize?, Phys. Rev. Lett. **121,** 085701 (2018).

[17] C.-J. Lin and O. I. Motrunich, Exact Quantum Many-Body Scar States in the Rydberg-Blockaded Atom Chain, Phys. Rev. Lett. **122,** 173401 (2019).

[18] M. Schecter and T. Iadecola, Weak Ergodicity Breaking and Quantum Many-Body Scars in Spin-1XY Magnets, Phys. Rev. Lett. **123,** 147201 (2019).

[19] S. Pai and M. Pretko, Dynamical Scar States in Driven Fracton Systems, Phys. Rev. Lett. **123,** 136401 (2019).

[20] H. Zhao, J. Vovrosh, F. Mintert, and J. Knolle, Quantum Many-Body Scars in Optical Lattices, Phys. Rev. Lett. **124,** 160604 (2020).

[21] H. Bernien, S. Schwartz, A. Keesling, H. Levine, A. Omran, H. Pichler, S. Choi, A. S. Zibrov, M. Endres, M. Greiner, V. Vuletić, and M. D. Lukin, Probing many-body dynamics on a 51-atom quantum simulator, Nature (London) **551,** 579 (2017).

[22] D. Bluvstein, A. Omran, H. Levine, A. Keesling, G. Semeghini, S. Ebadi, T. T. Wang, A. A. Michailidis, N. Maskara, W. W. Ho, S. Choi, M. Serbyn, M. Greiner, V. Vuletić, and M. D. Lukin, Controlling quantum many-body dynamics in driven Rydberg atom arrays, Science **371,** 1355 (2021).

[23] P. Sala, T. Rakovszky, R. Verresen, M. Knap, and F. Pollmann, Ergodicity Breaking Arising from Hilbert Space Fragmentation in Dipole-Conserving Hamiltonians, Phys. Rev. X **10,** 011047 (2020).

[24] V. Khemani, M. Hermele, and R. Nandkishore, Localization from Hilbert space shattering: From theory to physical realizations, Phys. Rev. B **101,** 174204 (2020).

[25] S. Moudgalya, A. Prem, R. Nandkishore, N. Regnault, and B. A. Bernevig, Thermalization and its absence within Krylov subspaces of a constrained Hamiltonian, Memorial Volume for Shoucheng Zhang 147–209 (2021) 10.1142/9789811231711_0009.

[26] S. Pai, M. Pretko, and R. M. Nandkishore, Localization in Fractonic Random Circuits, Phys. Rev. X **9,** 021003 (2019).

[27] S. R. Taylor, M. Schulz, F. Pollmann, and R. Moessner, Experimental probes of Stark many-body localization, Phys. Rev. B **102,** 054206 (2020).

[28] F. Ritort and P. Sollich, Glassy dynamics of kinetically constrained models, Adv. Phys. **52,** 219 (2003).

[29] N. Pancotti, G. Giudice, J. I. Cirac, J. P. Garrahan, and M. C. Bañuls, Quantum East Model: Localization, Nonthermal Eigenstates, and Slow Dynamics, Phys. Rev. X **10,** 021051 (2020).

[30] W. Morong, F. Liu, P. Becker, K. S. Collins, L. Feng, A. Kyprianidis, G. Pagano, T. You, A. V. Gorshkov, and C. Monroe, Observation of stark many-body localization without disorder, Nature (London) **599,** 393 (2021).

[31] Q. Guo, C. Cheng, H. Li, S. Xu, P. Zhang, Z. Wang, C. Song, W. Liu, W. Ren, H. Dong, R. Mondaini, and H. Wang, Stark Many-Body Localization on a Superconducting Quantum Processor, Phys. Rev. Lett. **127,** 240502 (2021).

[32] S. Scherg, T. Kohlert, P. Sala, F. Pollmann, B. H. M., I. Bloch, and M. Aidelsburger, Observing non-ergodicity due to kinetic constraints in tilted Fermi-Hubbard chains, Nat. Commun. **12,** 4490 (2021).

[33] See Supplemental Material at http://link.aps.org/supplemental/10.1103/PhysRevLett.130.010201, which includes Refs. [34–48], for details on: Experimental sequence, calibration and data acquisition techniques, initial state preparation and characterization, RF dressing, experimental imperfections, supplementary experimental data as well as details on analytical and numerical techniques (details on effective Hamiltonians, ED and TEBD simulations, Krylov methods and a quantitative analysis of experimental imperfections via an approximate method).

[34] U. Schneider, L. Hackermüller, S. Will, T. Best, I. Bloch, T. A. Costi, R. W. Helmes, D. Rasch, and A. Rosch, Metallic and insulating phases of repulsively interacting fermions in a 3D optical lattice, Science **522,** 1520 (2008).

[35] P. Bordia, H. P. Lüschen, S. S. Hodgman, M. Schreiber, I. Bloch, and U. Schneider, Coupling Identical One-dimensional Many-Body Localized Systems, Phys. Rev. Lett. **116,** 140401 (2016).

[36] J. Feldmann, K. Leo, J. Shah, D. A. B. Miller, J. E. Cunningham, T. Meier, G. von Plessen, A. Schulze, P. Thomas, and S. Schmitt-Rink, Optical investigation of Bloch oscillations in a semiconductor superlattice, Phys. Rev. B **46,** 7252(R) (1992).

[37] M. Ben Dahan, E. Peik, J. Reichel, Y. Castin, and C. Salomon, Bloch Oscillations of Atoms in an Optical Potential, Phys. Rev. Lett. **76,** 4508 (1996).

[38] J. Dalibard, Y. Castin, and K. Mølmer, Wave-Function Approach to Dissipative Processes in Quantum Optics, Phys. Rev. Lett. **68,** 580 (1992).

[39] H. J. Carmichael, Quantum Trajectory Theory for Cascaded Open Systems, Phys. Rev. Lett. **70,** 2273 (1993).

[40] M. H. Fischer, M. Maksymenko, and E. Altman, Dynamics of a Many-Body-Localized System Coupled to a Bath, Phys. Rev. Lett. **116,** 160401 (2016).

[41] U. Schneider, L. Hackermüller, J. P. Ronzheimer, S. Will, S. Braun, T. Best, I. Bloch, E. Demler, S. Mandt, D. Rasch, and A. Rosch, Fermionic transport and out-of-equilibrium dynamics in a homogeneous Hubbard model with ultracold atoms, Nat. Phys. **6,** 213 (2012).

[42] B. Hebbe Madhusudhana, S. Scherg, T. Kohlert, I.Bloch, and M. Aidelsburger, Benchmarking a novel efficient numerical method for localized field fermi-hubbard systems on a quantum simulator, PRX Quantum **2,** 040325 (2021).

[43] M. Lewenstein, A. Sanpera, and V. Ahufinger, *Ultracold Atoms in Optical Lattices* (Oxford University Press, 2021).

[44] D. Abanin, W. De Roeck, W. W. Ho, and F. Huveneers, A rigorous theory of many-body prethermalization for periodically driven and closed quantum systems, Commun. Math. Phys. **354,** 809 (2017).

[45] G. Vidal, Efficient Classical Simulation of Slightly Entangled Quantum Computations, Phys. Rev. Lett. **91,** 147902 (2003).

[46] D. V. Else, B. Bauer, and C. Nayak, Prethermal phases of matter protected by time-translation symmetry, Phys. Rev. X **7,** 011026 (2017).

[47] S. Bravyi, D. P. DiVincenzo, and D. Loss, Schrieffer-Wolff transformation for quantum many-body systems, Ann. Phys. **326,** 2793 (2011).

[48] M. T. DePue, C. McCormick, S. L. Winoto, S. Oliver, and D. S. Weiss, Unity Occupation of Sites in a 3D Optical Lattice, Phys. Rev. Lett. **82,** 2262 (1999).

[49] J. Sebby-Strabley, M. Anderlini, P. S. Jessen, and J. V. Porto, Lattice of double wells for manipulating pairs of cold atoms, Phys. Rev. A **73,** 033605 (2006).

[50] S. Fölling, S. Trotzky, P. Cheinet, M. Feld, R. Saers, A. Widera, T. Müller, and I. Bloch, Direct observation of second-order atom tunnelling, Nature (London) **448,** 1029 (2007).

[51] C. Skedrov, M. Menashes, G. Ness, A. Vainbaum, and Y. Sagi, Absence of Heating in a Uniform Fermi Gas Created by Periodic Driving, Phys. Rev. X **12,** 011041 (2022).

[52] S. Scherg, RF dressing with two-component fermions in optical lattices, Nat. Rev. Phys. **3,** 678 (2021).

[53] M. W. Zwierlein, Z. Hadzibabic, S. Gupta, and W. Ketterle, Spectroscopic Insensitivity to Cold Collisions in a Two-State Mixture of Fermions, Phys. Rev. Lett. **91,** 250404 (2003).

[54] S. Scherg, T. Kohlert, J. Herbrych, J. Stolpp, P. Bordia, U. Schneider, F. Heidrich-Meisner, I. Bloch, and M. Aidelsburger, Nonequilibrium Mass Transport in the 1D Fermi-Hubbard Model, Phys. Rev. Lett. **121,** 130402 (2018).

[55] F. Meinert, M. J. Mark, E. Kirilov, K. Lauber, P. Weinmann, M. Gröbner, A. J. Daley, and H.-C. Nägerl, Observation of many-body dynamics in long-range tunneling after a quantum quench, Science **344,** 1259 (2014).

[56] J.-Y. Desaules, A. Hudomal, C. J. Turner, and Z. Papić, A Proposal for Realizing Quantum Scars in the Tilted 1D Fermi-Hubbard Model, Phys. Rev. Lett. **126,** 210601 (2021).

[57] T. Rakovszky, P. Sala, R. Verresen, M. Knap, and F. Pollmann, Statistical localization: From strong fragmentation to strong edge modes, Phys. Rev. B **101,** 125126 (2020).

[58] M. Schulz, C. A. Hooley, R. Moessner, and F. Pollmann, Stark Many-Body Localization, Phys. Rev. Lett. **122,** 040606 (2019).

[59] E. van Nieuwenburg, Y. Baum, and G. Refael, From Bloch oscillations to many-body localization in clean interacting systems, Proc. Natl. Acad. Sci. U.S.A. **116,** 9269 (2019).

[60] E. Guardado-Sanchez, A. Morningstar, B. M. Spar, P. T. Brown, D. A. Huse, and W. S. Bakr, Subdiffusion and Heat Transport in a Tilted Two-Dimensional Fermi-Hubbard System, Phys. Rev. X **10,** 011042 (2020).

[61] J. Hauschild and F. Pollmann, Efficient numerical simulations with tensor networks: Tensor Network Python (TeNPy), SciPost Phys. Lect. Notes 5 (2018) 10.21468/SciPostPhysLectNotes.5.